Published in final edited form as:

Cell Rep. 2020 November 24; 33(8): 108408. doi:10.1016/j.celrep.2020.108408.

Transiently ‘‘Undead’’ Enterocytes Mediate Homeostatic Tissue Turnover in the Adult *Drosophila* Midgut

Alla Amcheslavsky[1], **Jillian L. Lindblad**[1], **Andreas Bergmann**[1,2,*]

[1]University of Massachusetts Medical School, Department of Molecular, Cell and Cancer Biology, Worcester, MA 01605, USA

[2]Lead Contact

SUMMARY

We reveal surprising similarities between homeostatic cell turnover in adult *Drosophila* midguts and ‘‘undead’’ apoptosis-induced compensatory proliferation (AiP) in imaginal discs. During undead AiP, immortalized cells signal for AiP, allowing its analysis. Critical for undead AiP is the Myo1D-dependent localization of the initiator caspase Dronc to the plasma membrane. Here, we show that Myo1D functions in mature enterocytes (ECs) to control mitotic activity of intestinal stem cells (ISCs). In *Myo1D* mutant midguts, many signaling events involved in AiP (ROS generation, hemocyte recruitment, and JNK signaling) are affected. Importantly, similar to AiP, *Myo1D* is required for membrane localization of Dronc in ECs. We propose that ECs destined to die transiently enter an undead-like state through Myo1D-dependent membrane localization of Dronc, which enables them to generate signals for ISC activity and their replacement. The concept of transiently ‘‘undead’’ cells may be relevant for other stem cell models in flies and mammals.

Graphical Abstract

*Correspondence: andreas.bergmann@umassmed.edu.

AUTHOR CONTRIBUTIONS

Conceptualization, A.A. and A.B.; Methodology, A.A.; Validation, A.A. and J.L.L.; Investigation, A.A. and J.L.L.; Writing – Original Draft, A.A. and A.B.; Writing – Review & Editing, A.B.; Visualization, A.A.; Supervision, A.B.; Funding Acquisition, A.B.

SUPPLEMENTAL INFORMATION

Supplemental Information can be found online at https://doi.org/10.1016/j.celrep.2020.108408.

DECLARATION OF INTERESTS

The authors declare no competing interests.

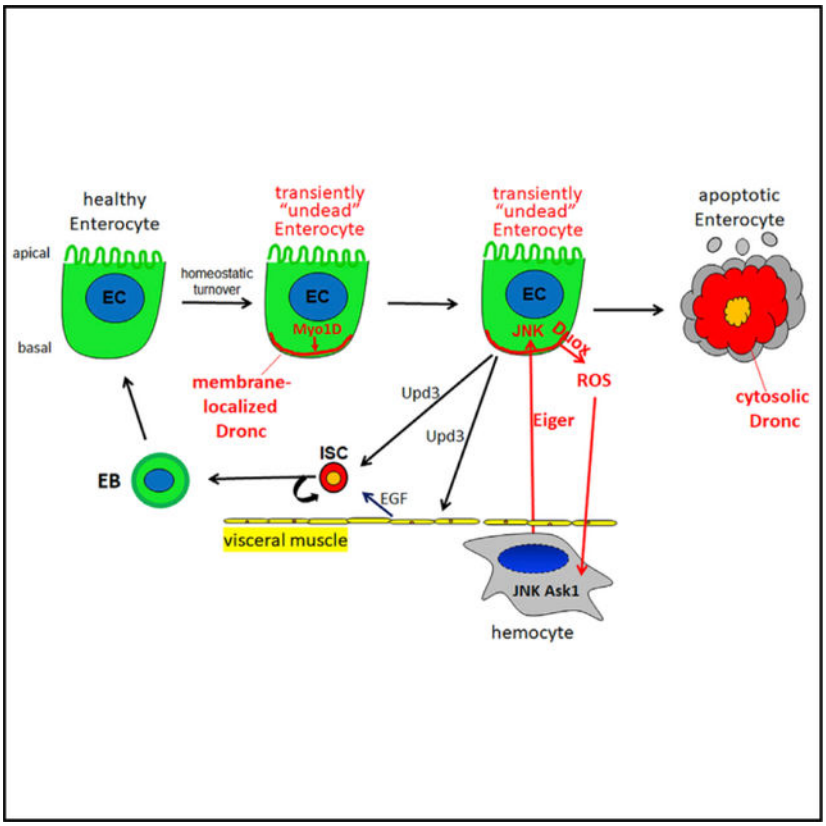

In Brief

Amcheslavsky et al. reveal a mechanism according to which apoptotic cells maintain survival transiently by entering an ‘‘undead’’-like state through membrane localization of Dronc in a Myo1D-dependent manner. This transient ‘‘undead’’-like state enables apoptotic cells for a short time to generate signals for mitotic activity of stem cells.

INTRODUCTION

Somatic stem cells maintain tissue homeostasis throughout the life of an animal. The rate of stem cell division, the differentiation of daughter cells, and the removal of differentiated cells have to be precisely controlled. Imbalance of this control can lead to premature aging and diseases such as cancer. The adult *Drosophila* posterior midgut, which is functionally equivalent to the mammalian small intestine, has become an important model for stem cell research (reviewed in Gervais and Bardin, 2017; Guo et al., 2016; Jiang and Edgar, 2011; Miguel-Aliaga et al., 2018). Particularly well studied are the regenerative responses due to infection by pathogenic bacteria and chemical damage (Lucchetta and Ohlstein, 2012). However, in addition to these regenerative responses and similar to mammalian intestines, there is normal homeostatic turnover of old absorptive enterocytes (ECs) and secretory enteroendocrine (EE) cells that need to be replaced by new, healthy cells. For example, the intestinal epithelium in the posterior midgut renews within 4 days (Liang et al., 2017). This is mediated through mitotic activity of intestinal stem cells (ISCs), the only mitotic cells in

the midgut, which asymmetrically divide to give rise to a new ISC and an enteroblast (EB) (Micchelli and Perrimon, 2006; Ohlstein and Spradling, 2006). Subsequently, the EB differentiates into an EC (Guo and Ohlstein, 2015; Ohlstein and Spradling, 2007). Topologically, ECs face the lumen of the gut with their apical side, while the basal side of ECs and progenitor cells (ISCs and EBs) are located basally and are in close contact with a group of visceral muscle cells, the circular muscles that surround the gut.

A large body of work has revealed the signaling mechanisms that control mitotic activity of ISCs. Upon bacterial infection or injury, signaling factors such as Unpaired 3 (Upd3) and the EGF ligands Keren (Krn) and Spitz (Spi) are released by ECs (Beebe et al., 2010; Biteau and Jasper, 2011; Buchon et al., 2010; Jiang and Edgar, 2009; Jiang et al., 2011, 2009; Lin et al., 2010; Osman et al., 2012; Xu et al., 2011). Upd3 stimulates Janus kinase/signal transducer and activator of transcription (Jak/STAT) signaling in ISCs and in the circular muscles (Zhou et al., 2013). The release of Upd3 requires the Jun N-terminal kinase (JNK) pathway in ECs (Jiang et al., 2009). Jak/STAT signaling in the circular muscle triggers the release of the EGF ligand Vein (Vn), which, together with EC-derived Krn and Spi, stimulates epidermal growth factor receptor (EGFR) activity in ISCs (Biteau et al., 2011; Biteau and Jasper, 2011). Circular muscle cells also secret Wingless (Wg) and Ilp3, which control Wg and Insulin signaling in ISCs (Choi et al., 2011; Gultekin and Steller, 2019; Lin et al., 2008; O'Brien et al., 2011; Tian et al., 2016). EBs release Upd and Upd2 as well as Spi (Jiang et al., 2011; Osman et al., 2012; Xu et al., 2011). Other signaling events involve Hippo and Dpp pathways (Ayyaz et al., 2015; Guo et al., 2013; Karpowicz et al., 2010; Li et al., 2013a, 2013b; Ren et al., 2010; Staley and Irvine, 2010; Tian and Jiang, 2014; Zhou et al., 2015). The combined activities of these signaling events control the mitotic activity of ISCs (reviewed in Gervais and Bardin, 2017; Guo et al., 2016). While most of these signaling events have been characterized under damaging and regenerative conditions, it is thought that they are also engaged for normal homeostatic turnover of the midgut at a lower level.

Nevertheless, at least for EC-derived Krn and Spi, a role in normal turnover of the midgut without damage has been demonstrated (Liang et al., 2017). First, it was demonstrated that EC apoptosis and mitotic activity of ISCs are homeostatically coupled to maintain tissue integrity (Liang et al., 2017). Second, mechanistically, in apoptotic ECs, the protease Rhomboid processes and activates Krn and Spi (Liang et al., 2017), which then stimulate EGFR signaling in ISCs. In this way, EC apoptosis and mitotic activity of ISCs are coupled and maintain homeostasis of the midgut.

In addition to these signaling events between different cell types in the midgut, *Drosophila* macrophages, termed hemocytes, are involved in the regulation of ISC activity in response to chemical and bacterial damage of the midgut (Ayyaz et al., 2015; Chakrabarti et al., 2016). They are the source of the signaling molecules Dpp and Upd3, which mediate the repair response. Whether hemocytes are also involved in normal gut turnover is less clear. Nevertheless, hemocytes are attached at normal midguts (Ayyaz et al., 2015; this study), making it possible that they are also part of the normal turnover process.

Despite this detailed knowledge about the signaling events between dying ECs and ISCs, there are still gaps in our understanding about the signaling events in ECs that are engaged

during normal turnover of the midgut. For example, is the aforementioned process of Rhomboid activation the only mechanism by which dying ECs control ISC activity? How is the release of other ligands such as Upd3 controlled? While JNK signaling induced by injury and bacterial infection is activated as part of a stress response (Lucchetta and Ohlstein, 2012), how is it activated for normal homeostatic turnover? Are hemocytes involved in regular EC turnover, and if so, what is their role in this process?

Usually, cells are eliminated by a regulated form of cell death, termed apoptosis (Fuchs and Steller, 2011). This requires the activity of a specific type of Cys-proteases known as caspases. There are two types of caspases: initiator caspases such as Caspase-9 and effector caspases such as Caspase-3 (Salvesen et al., 2016; Shalini et al., 2015). Initiator caspases cleave and activate effector caspases, which then mediate apoptosis. The major initiator caspase in *Drosophila* is the Caspase-9 ortholog Dronc, which cleaves and activates the effector caspases DrICE and Dcp1 to promote apoptosis (Fuchs and Steller, 2011; Salvesen et al., 2016; Shalini et al., 2015).

Dronc not only promotes apoptosis, but it also has non-apoptotic functions including apoptosis-induced compensatory proliferation (AiP), during which apoptotic cells are replaced by new cells (Fan and Bergmann, 2008; Mollereau et al., 2013). In order to examine AiP, we have been using the ‘‘undead’’ epithelial cell model in imaginal discs (Martín et al., 2009). In undead epithelial cells, the apoptotic pathway is induced by expression of upstream apoptotic regulators such as *reaper* or *hid* but is blocked downstream at the same time by the effector caspase inhibitor P35 that specifically inhibits DrICE and Dcp1, but not the initiator caspase Dronc. Thus, undead cells uncouple the functions of Dronc for apoptosis and AiP. As a result, apoptosis is blocked, but AiP still occurs resulting in hyperplasia of undead larval imaginal discs and overgrowth of adult appendages derived from these discs (Fan et al., 2014; Huh et al., 2004; Pérez-Garijo et al., 2004; Ryoo et al., 2004).

Using the undead AiP model in imaginal discs, we found that Dronc promotes the activation of the NADPH oxidase Duox, which produces extracellular reactive oxygen species (ROS). Hemocytes are attracted to undead tissue and release the tumor necrosis factor (TNF) ligand Eiger, which signals back to undead cells to stimulate JNK activity (Diwanji and Bergmann, 2020; Fogarty et al., 2016). JNK then promotes the release of mitogenic signaling molecules for AiP, most notably Wingless (Wg), Decapentaplegic (Dpp), and Spitz (Spi) (Fan et al., 2014; Huh et al., 2004; Pérez-Garijo et al., 2004; Ryoo et al., 2004; reviewed in Diwanji and Bergmann, 2019; Fogarty and Bergmann, 2017).

Recently, we reported another player in undead AiP, the unconventional Myosin 1D (Myo1D; aka Myo31DF) (Amcheslavsky et al., 2018). As a myosin, Myo1D contains an N-terminal head domain, a central neck domain with two IQ motifs, and a C-terminal tail domain (Barylko et al., 2000; Coluccio, 1997). It has been best studied for its function in left/right (L/R) asymmetry of certain visceral organs or for male genitalia rotation (Hozumi et al., 2006; Spéder et al., 2006). However, for undead AiP, Myo1D is required for the localization of Dronc to the plasma membrane, specifically the basal side of the plasma

membrane of epithelial disc cells where Dronc directly or indirectly activates Duox for ROS generation (Amcheslavsky et al., 2018).

Myo1D has long been known to be expressed in ECs of the midgut. A Gal4-enhancer trap insertion, *NP1-Gal4*, is under direct control of *Myo1D* regulatory sequences and is commonly used as a tool to express target genes, specifically in ECs in the midgut (Buchon et al., 2013; Jiang et al., 2009). This EC-specific expression of *Myo1D*, and our mechanistic finding that Dronc stimulates AiP in undead imaginal discs in a Myo1D-dependent manner, prompted us to examine if a similar signaling mechanism stimulates the mitotic activity of ISCs in the absence of P35.

Here, we present the analysis of the *Myo1D* mutant phenotype in the adult posterior midgut. Based on the *Myo1D* phenotype, we find that AiP signaling in undead imaginal discs and stimulation of mitotic activity of ISCs share many features. *Myo1D* mutants display reduced ISC activity. *Myo1D* is required for maintaining basal ROS levels in a Duox-dependent manner and the recruitment of hemocytes to the gut. Furthermore, ROS stimulate JNK activity in hemocytes and—mediated by Eiger—in ECs. Loss of *Myo1D* impairs Jak/STAT and EGFR signaling in ISCs and circular muscles. Mechanistically, similar to undead cells, *Myo1D* is required for localization of Dronc to the basal side of the EC plasma membrane, which is required for Duox activation. We propose that old ECs enter a transiently ‘‘undead’’-like state, which allows them to produce the signals for ISC activity before they become apoptotic and are removed.

RESULTS

Myo1D Is Non-Cell-Autonomously Required in Mature ECs to Maintain Mitotic Activity of ISCs in the Posterior Midgut

Because *Myo1D* is required for AiP in undead imaginal discs (Amcheslavsky et al., 2018) and is expressed in ECs (Jiang et al., 2009), we examined if *Myo1D* is involved in the control of mitotic activity of ISCs in the adult midgut using several well-characterized *Myo1D* mutant alleles. $Myo1D^{L152}$ carries a premature STOP codon at position 331 (Hozumi et al., 2006). $Myo1D^{K2}$ was obtained by imprecise excision of a P-allele and deletes almost the entire *Myo1D* locus (Spéder et al., 2006). $Myo1D^{EY08859}$ and *NP1-Gal4* carry P-element insertions immediately upstream of the transcriptional start site (FlyBase). In homozygous as well as trans-heterozygous *Myo1D* allelic combinations, the mitotic activity of ISCs is significantly reduced in adult midguts based on phospho-histone H3 (PH3) labeling experiments (Figure 1A). The Gal4-enhancer trap insertion in the *Myo1D* locus, *NP1-Gal4*, is also characterized by reduced mitotic activity (Figure 1A), suggesting that *NP1-Gal4* disrupts *Myo1D* function. Even heterozygous *Myo1D* mutant midguts showed a significant loss of ISC activity (Figure 1A).

To identify the cell type in which *Myo1D* is required for ISC mitotic activity, we expressed *Myo1D* RNAi using cell-type-specific Gal4 drivers. Downregulation of *Myo1D* in progenitor cells (ISCs and EBs) using *esg-Gal4* and *Su(H)-Gal4* did not result in significant loss of mitotic activity (Figure 1B). In contrast, EC-specific *Myo1D* RNAi by *NP1-Gal4* resulted in a strong reduction of ISC activity, similar to *Myo1D* mutants (Figures 1B–1D).

Consistently, overexpression of *Myo1D* in ECs, but not in ISCs or EBs, triggered a significant increase of mitotic activity in the midgut (Figures 1B and 1E). Similar results were obtained with an unrelated *Gal4* driver, the gene switch line *5966::GS* (Mathur et al., 2010; Morris et al., 2016), which is expressed in the EB/EC lineage (Figure 1B).

Next, we examined if expression of a wild-type *Myo1D* transgene can rescue the loss of ISC mitotic activity in *Myo1D* mutant midguts. Indeed, expression of *Myo1D* in ECs using *NP1-Gal4* restores the mitotic activity in *Myo1D* mutants approximately to normal levels (Figure 1F). Interestingly, overexpression of several transgenic *Myo1D* mutants affecting the head (*Myo1D*$^{-\Delta}$*Abs*), neck (*Myo1D*$^{\Delta IQ}$), and tail domains (*Myo1D*$^{\Delta tail}$) (Hozumi et al., 2008) using *NP1-Gal4* in otherwise wild-type background strongly lowered ISC activity in adult midguts (Figure 1G), suggesting that they behave as dominant-negative transgenes and further supporting the notion that *Myo1D* is required in ECs for ISC activity. Finally, the reduced mitotic activity of *Myo1D* mutants leads to a significant reduction in the number of ISCs and EBs based on *esg-lacZ* and *Su(H)-lacZ* labelings (Figures 1H–1L). EC-specific downregulation of *Myo1D* by RNAi confirms this result (Figures 1M–1Q). Together, these results demonstrate that *Myo1D* is non-autonomously required in mature ECs to maintain ISC activity and differentiation.

EC-Localized Myo1D Is Required for Jak/STAT Signaling in ISCs and EGF Expression in Circular Muscles

Next, we examined which signaling pathways may be affected by loss of *Myo1D*. We examined the expression levels of those ligands that have previously been implicated in mitotic activity of ISCs such as the Upd and EGF ligands in entire guts. Among the ligands tested, EC-specific knockdown of *Myo1D* has the most profound effect on the transcription of *upd*, *upd2*, and *upd3* (Figure 2A). Consistently, *Upd3-lacZ* expression is strongly reduced in midguts mutant for *Myo1D* or treated with EC-specific *Myo1D* knockdown (Figures 2B–2G). Furthermore, *STAT-GFP* expression, which is expressed in ISCs, is also strongly affected in *Myo1D* mutant midguts (Figures 2H and 2I; quantified in 2L), suggesting that *Myo1D* is required for Upd-mediated Jak/STAT signaling in ISCs.

Furthermore, Upd signaling also induces expression of the EGF ligand *vein* (*vn*) in circular muscles, which in turn induces EGFR activity in ISCs (Biteau and Jasper, 2011). Consistently, EGFR ligands (*spi*, *krn*, *vn*) are transcriptionally downregulated by EC-specific *Myo1D* RNAi (Figure 2A). In wild-type midguts, a *vn-lacZ* transgene induces β-Gal expression in nuclei of the circular muscle cells (Figures 2H′′ and 2J). This *vn-lacZ* expression is dependent on *Myo1D* (Figures 2I′′ and 2K; quantified in 2M and 2N). Furthermore, EC-specific overexpression of *Myo1D* increases *vn-lacZ* expression in circular muscles about 2-fold (Figures 2O and 2P; quantified in 2Q). In summary, these results strongly suggest that the reduced mitotic activity of ISCs in *Myo1D* mutant midguts (Figure 1A) is the result of impaired Upd and Jak/STAT signaling in ISCs as well as reduced EGF (Vn) signaling in circular muscle cells.

Myo1D Is Required for Basal Localization of the Initiator Caspase Dronc in ECs

In apoptotic cells, the initiator caspase Dronc is largely cytosolic. However, in undead imaginal disc cells, Dronc is localized at the basal side of the plasma membrane in a Myo1D-dependent manner (Amcheslavsky et al., 2018). At the plasma membrane, Dronc has a non-apoptotic function that culminates in Duox activation and ROS generation. We are using the basal membrane localization of Dronc as a marker of an undead-like condition.

We examined the subcellular localization of Dronc in cells of the adult midgut and focused either on the apical side, where the apical plasma membrane of ECs faces the lumen of the gut, or on the basal side of the midgut, where progenitor cells and the basal plasma membranes of ECs are localized (see schemes at the top of Figure 3). In wild-type midguts, little Dronc protein is detectable at the apical side of the midgut (Figure 3A). However, at the basal side of the midgut, Dronc protein is present in both progenitor cells and ECs (Figure 3B; blue arrowheads and white arrows, respectively). Interestingly, Dronc appears to be enriched at the membrane of many ECs (Figure 3B, white arrows; see another example in Figure S1). The enrichment of Dronc at the basal membrane of ECs is dependent on Myo1D, as *Myo1D* knockdown disrupts this localization pattern (Figures 3D and S1), while Dronc labeling remains unchanged in progenitor cells (Figure 3D, blue arrowheads). As expected, there is no labeling of Dronc at the apical side of ECs in *Myo1D* RNAi-expressing midguts (Figure 3C).

Dronc has also been observed at the plasma membrane in salivary glands, which is dependent on a factor called Tango7 (Kang et al., 2017). Therefore, we examined whether Tango7 has a role for membrane localization of Dronc in ECs. However, knockdown of *Tango7* does not mis-localize Dronc in adult midguts (Figure S1C), suggesting that Tango7 is not involved in Dronc localization in the adult midgut.

Intriguingly, not all ECs have membrane-localized Dronc. In some ECs, Dronc also has a cytosolic component (Figure 3B, yellow arrowheads). Consistently, cleaved caspase 3 (CC3) labeling, which is commonly used as an apoptotic marker, significantly overlaps with cytosolic Dronc in these ECs (Figures 3E–3E′′), suggesting that they are undergoing apoptosis. These results imply that similar to undead imaginal discs, one function of Myo1D in the adult midgut is to localize Dronc to the basal side of the plasma membrane of ECs. Because of these similarities, we postulate that ECs go through a transient ‘‘undead’’-like state before they become apoptotic and are removed from the gut. During the undead-like state, Myo1D localizes Dronc to the basal side of the plasma membrane and transiently diverts the apoptotic activity of Dronc to a non-apoptotic one. This conclusion raises the question of whether the loss of membrane-localization of Dronc in *Myo1D* mutant midguts causes increased caspase activity. We addressed this question using CaspaseTracker an *in vivo* caspase activity marker (Tang et al., 2015). There are indeed many additional cells in adult midguts with reduced *Myo1D* function that have increased CaspaseTracker activity (Figure S2), suggesting that Myo1D prevents caspases from being activated in these cells. It is unclear if these additional CaspaseTracker-positive cells correspond to undead-like cells in normal midguts because all markers of an undead-like state (such as membrane localization of Dronc) are lost in *Myo1D* mutant cells. Nevertheless, this analysis shows that Myo1D can contain caspase activity through membrane localization of Dronc.

In the following, we are examining the processes that are known to act downstream of Myo1D-dependent localization of Dronc in undead imaginal discs in the adult midgut, most notably ROS generation, hemocyte recruitment, and JNK activation (reviewed in Diwanji and Bergmann, 2019; Fogarty and Bergmann, 2017).

Myo1D Is Required for Maintaining Basal ROS Levels in ECs and Recruitment of Hemocytes

In undead imaginal discs, membrane-localized Dronc can stimulate the NADPH oxidase Duox to generate extracellular ROS in a Myo1D-dependent manner (Amcheslavsky et al., 2018). Therefore, we examined if Myo1D has a similar ROS-promoting function in the adult midgut using the *GstD-GFP* transgene as a redox reporter (Sykiotis and Bohmann, 2008). In wild-type midguts, there is strong activity of the *GstD-GFP* reporter (Figure 4A). Expression of the extracellular catalase IRC (immune-regulated catalase) in ECs reduces the *GstD-GFP* signal (Figure S3), suggesting that the *GstD-GFP* reporter can detect extracellular ROS. In *Myo1D* mutant midguts, there is a strong decrease in reporter activity (Figures 4A–4C). This activity of *Myo1D* is required in ECs, as EC-specific *Myo1D* RNAi resulted in strong downregulation of *GstD-GFP* expression (Figures 4D and 4E; quantified in 4I). Consistently, misexpression of *Myo1D* triggered increased GFP expression (Figures 4F and 4I). In contrast, misexpression of the dominant-negative transgenes $Myo1D^{\Delta IQ}$ and $Myo1D^{\Delta tail}$ resulted in loss of *GstD-GFP* expression (Figures 4G–4I). These results suggest that *Myo1D* is required for the generation of basal levels of ROS in the posterior midgut.

To identify the source of *Myo1D*-induced ROS, we considered that in undead imaginal discs, *Myo1D* promotes the activation of Duox for generation of ROS (Amcheslavsky et al., 2018) and took advantage of the observation that overexpression of *Myo1D* in ECs increases the mitotic activity of ISCs (Figure 1B). Indeed, EC-specific downregulation of *Duox* by RNAi strongly suppresses the increased mitotic activity of midguts misexpressing *Myo1D* (Figure 4J). To further confirm that extracellular ROS are required for mitotic activity of the midgut, we misexpressed the extracellular catalases IRC and hCatS in ECs (Ha et al., 2005a, 2005b). Both transgenes strongly suppressed the ectopic mitotic activity of *Myo1D*-overexpressing midguts (Figure 4J). Interestingly, while EC-specific misexpression of *Duox* in otherwise wild-type midguts cannot stimulate ISC activity, the same treatment can partially rescue the loss of mitotic activity of *Myo1D*-RNAi-expressing midguts (Figure 4K), suggesting the *Duox* acts genetically downstream of *Myo1D*, consistent with the data in undead imaginal discs (Amcheslavsky et al., 2018).

In undead imaginal discs, extracellular ROS directly or indirectly attract and activate hemocytes (Fogarty et al., 2016). It was previously shown that hemocytes are attached to and influence the behavior of adult midguts (Ayyaz et al., 2015; Chakrabarti et al., 2016). In particular, they cluster in folds of the middle midgut (Ayyaz et al., 2015) but are also attached in smaller numbers along the posterior midgut. In this paper, we characterize the attachment of hemocytes to the posterior midgut. Reduction of *Myo1D* activity by RNAi results in partial loss of attached hemocytes along the posterior midgut (Figures 4L, 4M, and 4P). This recruitment of hemocytes to the adult midgut is dependent on ROS, as *Duox* RNAi

or expression of the secreted catalase *hCatS* significantly reduces the number of attached hemocytes (Figures 4N and 4O; quantified in 4P).

One mechanism by which ROS can mediate redox signaling is through activation of the JNKKK Ask1 and, subsequently, JNK (Muzzopappa et al., 2017; Patel et al., 2019; Ray et al., 2012; Santabárbara-Ruiz et al., 2019). We examined if a similar mechanism operates in hemocytes. Consistently, downregulation of *Ask1* specifically in hemocytes using *hmlΔ-Gal4* results in a significant reduction of mitotic activity in the adult midgut (Figure 5A). Consistently, we observe JNK activity in hemocytes using *puc-lacZ* as JNK marker (Figure 5B). This hemocyte-specific JNK activity is partially dependent on Ask1 because knockdown of *Ask1* results in partial loss of JNK activity (Figure 5C; quantified in 5D).

We observed JNK activity not only in hemocytes, but also in ECs (Figure 5E), which are dependent on *Myo1D* (Figure S4). Interestingly, hemocyte-specific loss of JNK activity by *Ask1* RNAi causes a weak but significant reduction of JNK activity in ECs (Figure 5F; quantified in 5G), suggesting that ROS-mediated JNK activation in hemocytes at least partially also triggers JNK signaling in ECs. In the undead imaginal disc model, we identified the TNF ortholog Eiger as a hemocyte-derived signal for JNK activation (Fogarty et al., 2016). Consistently, hemocyte-specific RNAi of *Eiger* leads to a weak, but significant, reduction of JNK activity in ECs (Figures 5H–5J) and reduced mitotic activity of the midgut (Figure 5K). Furthermore, hemocyte-specific overexpression of *Eiger* resulted in strong activation of mitotic activity in the midgut (Figure 5K). Together, these results suggest that ROS from ECs trigger JNK activation in hemocytes, followed by hemocyte-dependent release of Eiger, which promotes JNK activation in ECs.

DISCUSSION

By examining the mutant phenotype of the unconventional myosin, *Myo1D*, we reveal significant similarities between AiP in undead larval imaginal disc cells and the control of mitotic stem cell (ISC) activity in the adult posterior midgut (see comparisons of both systems in Figures 6A and 6B). *Myo1D* is required non-autonomously in ECs for a significant fraction of the mitotic activity of ISCs (Figure 1A). Loss of *Myo1D* affects the signaling pathways (Jak/STAT and EGFR), which are required for ISC activity. Mechanistically, Myo1D is required for localization of the initiator caspase Dronc to the basal side of the plasma membrane of ECs. This basal localization is critical for cell-cell communication in the gut because ISCs and circular muscle cells are located at the basal surface of the gut. Furthermore, hemocytes also attach to the midgut at the basal side (Figure 6B). At the basal side of ECs, Dronc directly or indirectly activates Duox for ROS generation, which attracts hemocytes and promotes JNK activity in hemocytes. Finally, hemocyte-specific release of Eiger maintains JNK activity in ECs.

Because of these similarities between undead AiP and control of ISC activity in the adult midgut, we propose that old ECs enter into a transiently ‘‘undead’’-like state, which allows them to produce the signals for ISC activity before they become apoptotic and are removed (Figure 6B). Once enough signal (ROS) is produced by the Dronc/Duox interaction at the basal side, ECs lose the undead state, release Dronc from the plasma membrane into the

cytosol, and undergo apoptosis (Figure 6B). A challenge in the future will be to determine how Myo1D becomes activated for membrane localization of Dronc in aging ECs.

According to this model, we would posit that EC-specific loss of *Dronc* would at least partially block ISC proliferation. Unfortunately, while EC-specific *Dronc* knockdown indeed reduces the amount of ISC proliferation, the results were statistically not significant (Figure S5). We also observed an upregulation of mitotic activity in response to *Dronc* overexpression. Again, while the trend of these data is in the right direction, this upregulation is statistically not significant (Figure S5). Nevertheless, despite these disappointing data, they do teach us an important lesson. Under the ideal, straightforward conditions in the undead *hid,p35*-expressing AiP model in imaginal discs, Dronc has by default a very important role due to the inhibition of effector caspases by P35, and hence, undead AiP is very dependent on Dronc. However, under more natural conditions such as the EC turnover in the intestine, the transiently undead-like condition may require not only Dronc, but potentially also other caspases including effector caspases. Nevertheless, characterizing the undead AiP model in imaginal discs identified genes and markers such as the membrane-localization of Dronc, which are useful tools for the study of natural AiP such as EC turnover in the adult midgut.

In this context, it is interesting to note that misexpression of the effector caspase inhibitor p35 in ECs does not generate or extend the undead-like condition of ECs and does not trigger hyperplasia of ISCs (Liang et al., 2017). There are at least two reasons for this observation. First, not every cell type responds to an induced undead-like condition by triggering hyperplasia as do epithelial cells in imaginal discs. For example, co-expression of *hid* and *p35* in neurons or glia does not induce hyperplasia. Second, the removal of dying ECs and proliferation of ISCs are strictly coupled (Liang et al., 2017). Therefore, because p35 expression blocks EC apoptosis, it will also block ISC proliferation. Thus, even though we postulate here that ECs undergo an intrinsic transient undead-like state, this state cannot be extended by overexpression of p35, suggesting that the undead condition of ECs is p35-independent.

The concept of a transiently undead-like state may not be limited to the homeostatic turnover in the posterior midgut in *Drosophila*. It is possible that tissues that undergo regular cellular turnover use a similar mechanism to stimulate stem cell activity. An undead-like condition will ensure that cells destined to die can still signal for their own replacement before they are irreversibly removed. This may be the case not only in *Drosophila*, but also in mammals including humans. Future work will reveal how applicable this concept is for control of stem cell activity in other tissues and organisms.

Although *Myo1D* is required for a significant fraction of ISC mitotic activity, even in null mutants, ISC activity is not completely blocked, suggesting that there are other mechanisms operating in ECs that control ISC activity. Indeed, at least one other mechanism has been reported (Liang et al., 2017). This mechanism, which controls the release of EC-derived EGF ligands Krn and Spi, centers on the expression of *rhomboid*, which encodes a protease for maturation of Krn and Spi. These ligands then stimulate the EGFR on ISCs for mitotic activity (Liang et al., 2017). Therefore, while the Rhomboid-dependent mechanism controls

the activation of Krn and Spi, our data suggest that the release of Upd3 and potentially other ligands from ECs depends on Myo1D. Combined, these activities control the mitotic activity of ISC and ensure steady-state turnover of the midgut.

The concept of an undead-like, p35-independent state has also been put forward in the context of tumorigenesis in *Drosophila*. However, in this pathologic condition, the undead-like state allows tumor cells to escape the apoptotic activity of caspases permanently. This was first reported in a *csk*,Ras^{V12} tumor model in *Drosophila* (Hirabayashi et al., 2013). More recently, we reported a similar undead-like behavior of neoplastic *scrib*,Ras^{V12} tumor cells (Pérez et al., 2017). Because these tumor cells do not express p35, it is possible that oncogenes such as Ras^{V12} mediate the undead-like state. Ras^{V12}, which possesses anti-apoptotic properties (Bergmann et al., 1998, 2002; Kurada and White, 1998), keeps caspase activity low in tumor cells and diverts their cell killing function to the generation of ROS in a Duox-dependent manner (Pérez et al., 2017). We also observed a Myo1D-dependent membrane localization of Dronc in *scrib*,Ras^{V12} tumor cells (Amcheslavsky et al., 2018). Therefore, membrane localization of Dronc appears to be an important step for cells to achieve an undead-like state. It is possible that other developmental, homeostatic, and pathological events also require membrane localization of Dronc or other caspases for additional non-apoptotic functions.

ROS are usually considered to be damaging agents for cellular components such as DNA, proteins, lipids, and more. In case of the anti-bacterial effect of ROS in the gut lumen, this is certainly the case. However, ROS can also mediate controlled signaling functions (Ray et al., 2012; Schieber and Chandel, 2014). For example, by redox signaling, ROS can promote JNK activation (Ray et al., 2012; Santabárbara-Ruiz et al., 2019). That appears to be the case for JNK activation in hemocytes attached to the midgut. A redox-sensitive component in the JNK pathway is the JNKKK Ask1 (Ray et al., 2012; Santabárbara-Ruiz et al., 2019). Consistently, downregulation of *Ask1* results in partial loss of ISC activity (Figure 5A), suggesting that Duox-generated ROS in ECs may trigger JNK activation through activation of Ask1 in hemocytes. Interestingly, JNK activation is detectable not only in hemocytes, but also in ECs. JNK activation in ECs is mediated through hemocyte-specific release of Eiger, as *Eiger* RNAi in hemocytes reduces JNK activity in ECs and mitotic activity of ISCs (Figures 5I–5K). In summary, it appears that ROS trigger JNK activation in hemocytes directly and in ECs indirectly.

In conclusion, we propose that old ECs enter a transiently undead-like condition to enable cell-cell communication for stimulation of ISC mitosis before they are removed from the gut epithelium. Such a mechanism ensures that ISC activity is only induced when new cells are needed and thus promotes tissue homeostasis. The unconventional myosin Myo1D plays a key role in this process. Future work will address the questions of when and how Myo1D becomes activated for localization of Dronc to the basal side of the plasma membrane. It will also be important to determine the mechanism that releases Dronc from the plasma membrane once enough signal has been generated for ISC activity. Furthermore, how Dronc activates the NAPDH oxidase Duox for ROS production is another important question. It is possible that the concept of transiently ‘‘undead’’ cells is of relevance for other stem cell models in flies and other organisms including humans.

STAR★METHODS

RESOURCE AVAILABILITY

Lead Contact—Further information and requests for resources and reagents should be directed to and will be fulfilled by the Lead Contact, Andreas Bergmann (andreas.bergmann@umassmed.edu).

Materials Availability—All unique/stable materials generated in this study is available from the Lead Contact without restriction.

Data and Code Availability—This study did not generate any unique datasets or code.

EXPERIMENTAL MODEL AND SUBJECT DETAILS

The experimental model organism is *Drosophila melanogaster*. Details of genotypes used in this study and their sources are described in the Key Resources Table. All crosses were performed on standard cornmeal-molasses medium (60 g/L cornmeal, 60ml/L molasses, 23.5g/L bakers yeast, 6.5g/L agar, 4ml/L acid mix and 0.13% Tegosept). Crosses not involving conditional expression of transgenes were incubated at room temperature. Crosses involving conditional *Gal80^{ts}*-dependent expression of transgenes including RNAi were incubated at 18°C until adult offspring eclosed. Adults were kept at 18°C for 5–6 days before they were incubated at 29°C for another 6–7 days prior to dissection. Expression of the gene switch Gal4 line *5966::GS* was induced according to Morris et al. (2016). 5–6 days old adult flies were transferred onto RU-486 containing fly food (0.2mg/ml) and incubated for another 5–6 days at 29°C. Flies were provided fresh food supplemented with yeast poweder every 2 days. Only female midguts were dissected and analyzed.

METHOD DETAILS

Fly stocks and genetics—Flies (*Drosophila melanogaster*) were reared on standard cornmeal-molasses medium. The Gal4-UAS system was used to express transgenes of interest in specific cell types of the midgut. *tub-Gal80^{ts}* or the gene-switch Gal4 line *5966::GS* were used for conditional expression of transgenes. *w^{1118}*, *UAS-mCD8GFP* in *w^{1118}* background and *UAS-RFP* RNAi were used as control stocks. The stocks used in this study are listed in the Key Resources Table (KRT).

The following *Myo1D* stocks were used: *Myo1D^{L152}* (Hozumi et al., 2006); *Myo1D^{K2}* (Spéder et al., 2006); *Myo1D^{EY08859}* (BDSC19940); *UAS-Myo1D*, *UAS-Myo1D$^{\Delta Abs}$*, *UAS-Myo1D$^{\Delta IQ}$* and *UAS-Myo1D$^{\Delta tail}$* (Hozumi et al., 2008); *UAS-Myo1D* RNAi (BDSC33971 and v102456). Other stocks used were: *esg-Gal4* (Yagi and Hayashi, 1997); *Su(H)-Gal4* (Zeng et al., 2010); *NP1-Gal4* (Jiang et al., 2009); 5966::GS (Mathur et al., 2010); *Su(H)-lacZ* = *Su(H)GBE-lacZ* (Furriols and Bray, 2001); *hmlΔ-Gal4* (Sinenko and Mathey-Prevot, 2004); *hmlΔ-DsRed* (Makhijani et al., 2011); *esg-lacZ* (BDSC67748); *GstD-GFP* (Sykiotis and Bohmann, 2008); CaspaseTracker combined with GTRACE (Tang et al., 2015); *TRE-RFP* (Chatterjee and Bohmann, 2012); *msn-lacZ* = *msn^{06946}* (BDSC11707); *upd3-lacZ* (Zhou et al., 2013); *STAT-GFP* (Bach et al., 2007); *vn-lacZ* (BL11749); *UAS-duox* RNAi, *UAS-IRC* and *UAS-hCatS* (Ha et al., 2005b); *UAS-Ask1*

RNAi (BDSC32464); *UAS-Eiger* RNAi (Igaki et al., 2002); *UAS-Dronc* RNAi (VDRC P {KK104278}v100424); *UAS-Dronc* (Kamber Kaya et al., 2017); *tub-Gal80^{ts}* (McGuire et al., 2003).

Dissection and immunolabeling of adult guts—Intact female midguts were dissected using standard protocols (Amcheslavsky et al., 2009). Primary antibodies were: PH3 (Millipore: 1:2,000), β-Galactosidase (DSHB; 1:100 (concentrate)), NimC (Kurucz et al., 2007; 1:300); Dronc (SK11) (Wilson et al., 2002; 1:200); cleaved caspase 3 (CC3) (Cell Signaling Technology; 1:400). Secondary antibodies were donkey Fab fragments from Jackson ImmunoResearch. If not noted otherwise, region R4ab in the posterior midgut was imaged and analyzed. Images were obtained with a Zeiss LSM 700 confocal microscope, analyzed with Zen 2012 imaging software (Carl Zeiss) and processed with Adobe Photoshop CS6.

qRT-PCR—Total RNA from 10 adult midguts was isolated using Trizol (Invitrogen). cDNA was synthesized from 1 μg of RNA with the QuantiTect Reverse Transcription Kit (QIAGEN). For RT-PCR analysis, 50 ng of cDNA per reaction was subjected to 40 amplification cycles. Realtime quantification was performed using Power SYBR green PCR Master Mix reagents (Applied Biosystems) on QuantStudio 6 Flex Real-Time PCR System (Applied Biosystem) according to the manufacturer's instructions. *rp49* expression was used as an internal control for normalization. Three experiments for each genotype were averaged.

Sequences for isoform-specific primers are listed in Table S1.

QUANTIFICATION AND STATISTICAL ANALYSIS

Counts and analysis of PH3- and lacZ-positive cells and hemocytes attached to the midgut—Total number of PH3-, *esg-lacZ*-, *Su(H)-lacZ*-positive cells and hemocytes (*hmlΔ-DsRed*) attached to the midguts were counted manually by detecting signal-positive cells as spots. At least three independent experiments for every genotype were performed. Analysis and graph generation was done using GraphPad Prism 7.04. The statistical method used is indicated in the legends to the respective panels. Plotted is mean intensity ± SEM. P values: * $p < 0.05$; ** $p < 0.01$; *** $p < 0.001$; **** $p < 0.0001$.

QUANTIFICATION OF CONFOCAL IMAGES

For quantification of confocal images, the 'Record Measurement' function of Photoshop was used. Discs were outlined and signal intensity was determined. Crosses were repeated at least three times. Analysis and graph generation was done using GraphPad Prism 7.04. The statistical method used is indicated in the legends to the respective panels. Plotted is mean intensity ± SEM. P values: * $p < 0.05$; ** $p < 0.01$; *** $p < 0.001$; **** $p < 0.0001$.

N numbers are as follows:

Figure 1A: n = 9, 9, 8, 11, 9, 11, 9, 10, 12 (from left to right).

Figure 1B: n = 26, 24, 24, 9, 9, 7, 36, 35, 28, 15, 15, 15 (from left to right).

Figure 1F: n = 12, 12, 15, 10, 12, 9, 9 (from left to right).

Figure 1G: n = 9, 9, 9, 9 (from left to right).

Figure 1L: n = 6, 5, 7, 4 (from left to right).

Figure 1Q: n = 4, 4, 5, 4 (from left to right).

Figure 2D: n=6 (w^{1118}), 4 ($Myo1D^{L152}/+$).

Figure 2G: n = 3 (ctrl), 3 (*Myo1D* RNAi).

Figure 2L: n= 5 (w^{1118}), 3 ($Myo1D^{L152}/+$).

Figure 2M: n = 30 (w^{1118}), 21 ($Myo1D^{L152}/+$).

Figure 2N: n = 24 (ctrl), 28 (*Myo1D* RNAi).

Figure 2Q: n = 14 (ctrl), 38 (*UAS-Myo1D*).

Figure 4C: n = 45 (w^{1118}) and 41 ($Myo1D^{L152}/+$).

Figure 4I: n = 40, 46, 45, 44, 44 (from left to right).

Figure 4J: n = 20, 30, 12, 10 (from left to right).

Figure 4K: n = 12, 11, 11, 8 (from left to right).

Figure 4P: n = 24, 19, 26, 20 (from left to right).

Figure 5A: n = 41 (ctrl), 39 ($Ask1^{RNAi}$).

Figure 5D: n = 4 (ctrl), 4 ($Ask1^{RNAi}$).

Figure 5G: n = 8 (ctrl), 8 ($Ask1^{RNAi}$).

Figure 5J: n = 3 (ctrl), 3 ($eiger^{RNAi}$).

Figure 5K: n = 23 (ctrl), 15 ($eiger^{RNAi}$), 31 (*UAS-eiger*).

Supplementary Material

Refer to Web version on PubMed Central for supplementary material.

ACKNOWLEDGMENTS

We would like to thank István Andó, Katja Brückner, Marie Hardwick, Y. Tony Ip, Won Jae Lee, Kenji Matsuno, Pascal Meier, Masayuki Miura, Stéphane Noselli, Benjamin Ohlstein, the Bloomington *Drosophila* Stock Center (BDSC), the Vienna *Drosophila* Resource Center (VDRC), and the Developmental Studies Hybridoma Bank (DSHB) for reagents, fly stocks, and antibodies. This work was funded by the National Institute of General Medical Sciences (NIGMS) under award R35GM118330. The content is solely the responsibility of the authors and does not necessarily represent the official views of the NIH.

REFERENCES

Amcheslavsky A, Jiang J, and Ip YT (2009). Tissue damage-induced intestinal stem cell division in Drosophila. Cell Stem Cell 4, 49–61. [PubMed: 19128792]

Amcheslavsky A, Wang S, Fogarty CE, Lindblad JL, Fan Y, and Bergmann A (2018). Plasma Membrane Localization of Apoptotic Caspases for Non-apoptotic Functions. Dev. Cell 45, 450–464.e453. [PubMed: 29787709]

Ayyaz A, Li H, and Jasper H (2015). Haemocytes control stem cell activity in the Drosophila intestine. Nat. Cell Biol 17, 736–748. [PubMed: 26005834]

Bach EA, Ekas LA, Ayala-Camargo A, Flaherty MS, Lee H, Perrimon N, and Baeg GH (2007). GFP reporters detect the activation of the Drosophila JAK/STAT pathway in vivo. Gene Expr. Patterns 7, 323–331. [PubMed: 17008134]

Barylko B, Binns DD, and Albanesi JP (2000). Regulation of the enzymatic and motor activities of myosin I. Biochim. Biophys. Acta 1496, 23–35. [PubMed: 10722874]

Beebe K, Lee WC, and Micchelli CA (2010). JAK/STAT signaling coordinates stem cell proliferation and multilineage differentiation in the Drosophila intestinal stem cell lineage. Dev. Biol. 338, 28–37. [PubMed: 19896937]

Bergmann A, Agapite J, McCall K, and Steller H (1998). The Drosophila gene hid is a direct molecular target of Ras-dependent survival signaling. Cell 95, 331–341. [PubMed: 9814704]

Bergmann A, Tugentman M, Shilo BZ, and Steller H (2002). Regulation of cell number by MAPK-dependent control of apoptosis: a mechanism for trophic survival signaling. Dev. Cell 2, 159–170. [PubMed: 11832242]

Biteau B, and Jasper H (2011). EGF signaling regulates the proliferation of intestinal stem cells in Drosophila. Development 138, 1045–1055. [PubMed: 21307097]

Biteau B, Hochmuth CE, and Jasper H (2011). Maintaining tissue homeostasis: dynamic control of somatic stem cell activity. Cell Stem Cell 9, 402–411. [PubMed: 22056138]

Buchon N, Broderick NA, Kuraishi T, and Lemaitre B (2010). Drosophila EGFR pathway coordinates stem cell proliferation and gut remodeling following infection. BMC Biol 8, 152. [PubMed: 21176204]

Buchon N, Osman D, David FP, Fang HY, Boquete JP, Deplancke B, and Lemaitre B (2013). Morphological and molecular characterization of adult midgut compartmentalization in Drosophila. Cell Rep 3, 1725–1738. [PubMed: 23643535]

Chakrabarti S, Dudzic JP, Li X, Collas EJ, Boquete JP, and Lemaitre B (2016). Remote Control of Intestinal Stem Cell Activity by Haemocytes in Drosophila. PLoS Genet 12, e1006089. [PubMed: 27231872]

Chatterjee N, and Bohmann D (2012). A versatile FC31 based reporter system for measuring AP-1 and Nrf2 signaling in Drosophila and in tissue culture. PLoS ONE 7, e34063. [PubMed: 22509270]

Choi NH, Lucchetta E, and Ohlstein B (2011). Nonautonomous regulation of Drosophila midgut stem cell proliferation by the insulin-signaling pathway. Proc. Natl. Acad. Sci. USA 108, 18702–18707. [PubMed: 22049341]

Coluccio LM (1997). Myosin I. Am. J. Physiol 273, C347–C359. [PubMed: 9277333]

Diwanji N, and Bergmann A (2019). Two Sides of the Same Coin - Compensatory Proliferation in Regeneration and Cancer. Adv. Exp. Med. Biol 1167, 65–85. [PubMed: 31520349]

Diwanji N, and Bergmann A (2020). Basement membrane damage by ROS- and JNK-mediated Mmp2 activation drives macrophage recruitment to overgrown tissue. Nat. Commun 11, 3631. [PubMed: 32686670]

Fan Y, and Bergmann A (2008). Apoptosis-induced compensatory proliferation. The Cell is dead. Long live the Cell!. Trends Cell Biol 18, 467–473. [PubMed: 18774295]

Fan Y, Wang S, Hernandez J, Yenigun VB, Hertlein G, Fogarty CE, Lindblad JL, and Bergmann A (2014). Genetic models of apoptosis-induced proliferation decipher activation of JNK and identify a requirement of EGFR signaling for tissue regenerative responses in Drosophila. PLoS Genet 10, e1004131. [PubMed: 24497843]

Fogarty CE, and Bergmann A (2017). Killers creating new life: caspases drive apoptosis-induced proliferation in tissue repair and disease. Cell Death Differ 24, 1390–1400. [PubMed: 28362431]

Fogarty CE, Diwanji N, Lindblad JL, Tare M, Amcheslavsky A, Makhijani K, Brückner K, Fan Y, and Bergmann A (2016). Extracellular Reactive Oxygen Species Drive Apoptosis-Induced Proliferation via Drosophila Macrophages. Curr. Biol 26, 575–584. [PubMed: 26898463]

Fuchs Y, and Steller H (2011). Programmed cell death in animal development and disease. Cell 147, 742–758. [PubMed: 22078876]

Furriols M, and Bray S (2001). A model Notch response element detects Suppressor of Hairless-dependent molecular switch. Curr. Biol 11, 60–64. [PubMed: 11166182]

Gervais L, and Bardin AJ (2017). Tissue homeostasis and aging: new insight from the fly intestine. Curr. Opin. Cell Biol 48, 97–105. [PubMed: 28719867]

Gultekin Y, and Steller H (2019). Axin proteolysis by Iduna is required for the regulation of stem cell proliferation and intestinal homeostasis in *Drosophila*. Development 146, dev169284.

Guo Z, and Ohlstein B (2015). Stem cell regulation. Bidirectional Notch signaling regulates Drosophila intestinal stem cell multipotency. Science 350, aab0988.

Guo Z, Driver I, and Ohlstein B (2013). Injury-induced BMP signaling negatively regulates Drosophila midgut homeostasis. J. Cell Biol 201, 945–961. [PubMed: 23733344]

Guo Z, Lucchetta E, Rafel N, and Ohlstein B (2016). Maintenance of the adult Drosophila intestine: all roads lead to homeostasis. Curr. Opin. Genet. Dev 40, 81–86. [PubMed: 27392294]

Ha EM, Oh CT, Bae YS, and Lee WJ (2005a). A direct role for dual oxidase in Drosophila gut immunity. Science 310, 847–850. [PubMed: 16272120]

Ha EM, Oh CT, Ryu JH, Bae YS, Kang SW, Jang IH, Brey PT, and Lee WJ (2005b). An antioxidant system required for host protection against gut infection in Drosophila. Dev. Cell 8, 125–132. [PubMed: 15621536]

Hirabayashi S, Baranski TJ, and Cagan RL (2013). Transformed Drosophila cells evade diet-mediated insulin resistance through wingless signaling. Cell 154, 664–675. [PubMed: 23911328]

Hozumi S, Maeda R, Taniguchi K, Kanai M, Shirakabe S, Sasamura T, Spéder P, Noselli S, Aigaki T, Murakami R, and Matsuno K (2006). An unconventional myosin in Drosophila reverses the default handedness in visceral organs. Nature 440, 798–802. [PubMed: 16598258]

Hozumi S, Maeda R, Taniguchi-Kanai M, Okumura T, Taniguchi K, Kawakatsu Y, Nakazawa N, Hatori R, and Matsuno K (2008). Head region of unconventional myosin I family members is responsible for the organ-specificity of their roles in left-right polarity in Drosophila. Dev. Dyn 237, 3528–3537. [PubMed: 18521948]

Huh JR, Guo M, and Hay BA (2004). Compensatory proliferation induced by cell death in the Drosophila wing disc requires activity of the apical cell death caspase Dronc in a nonapoptotic role. Curr. Biol 14, 1262–1266. [PubMed: 15268856]

Igaki T, Kanda H, Yamamoto-Goto Y, Kanuka H, Kuranaga E, Aigaki T, and Miura M (2002). Eiger, a TNF superfamily ligand that triggers the Drosophila JNK pathway. EMBO J 21, 3009–3018. [PubMed: 12065414]

Jiang H, and Edgar BA (2009). EGFR signaling regulates the proliferation of Drosophila adult midgut progenitors. Development 136, 483–493. [PubMed: 19141677]

Jiang H, and Edgar BA (2011). Intestinal stem cells in the adult Drosophila midgut. Exp. Cell Res 317, 2780–2788. [PubMed: 21856297]

Jiang H, Patel PH, Kohlmaier A, Grenley MO, McEwen DG, and Edgar BA (2009). Cytokine/Jak/Stat signaling mediates regeneration and homeostasis in the Drosophila midgut. Cell 137, 1343–1355. [PubMed: 19563763]

Jiang H, Grenley MO, Bravo MJ, Blumhagen RZ, and Edgar BA (2011). EGFR/Ras/MAPK signaling mediates adult midgut epithelial homeostasis and regeneration in Drosophila. Cell Stem Cell 8, 84–95. [PubMed: 21167805]

Kamber Kaya HE, Ditzel M, Meier P, and Bergmann A (2017). An inhibitory mono-ubiquitylation of the Drosophila initiator caspase Dronc functions in both apoptotic and non-apoptotic pathways. PLoS Genet 13, e1006438. [PubMed: 28207763]

Kang Y, Neuman SD, and Bashirullah A (2017). Tango7 regulates cortical activity of caspases during reaper-triggered changes in tissue elasticity. Nat. Commun 8, 603. [PubMed: 28928435]

Karpowicz P, Perez J, and Perrimon N (2010). The Hippo tumor suppressor pathway regulates intestinal stem cell regeneration. Development 137, 4135–4145. [PubMed: 21098564]

Kurada P, and White K (1998). Ras promotes cell survival in Drosophila by downregulating hid expression. Cell 95, 319–329. [PubMed: 9814703]

Kurucz E, Vaczi B, Markus R, Laurinyecz B, Vilmos P, Zsamboki J, Csorba K, Gateff E, Hultmark D, and Ando I (2007). Definition of Drosophila hemocyte subsets by cell-type specific antigens. Acta biologica Hungarica 58, 95–111. [PubMed: 18297797]

Li H, Qi Y, and Jasper H (2013a). Dpp signaling determines regional stem cell identity in the regenerating adult Drosophila gastrointestinal tract. Cell Rep 4, 10–18. [PubMed: 23810561]

Li Z, Zhang Y, Han L, Shi L, and Lin X (2013b). Trachea-derived dpp controls adult midgut homeostasis in Drosophila. Dev. Cell 24, 133–143. [PubMed: 23369712]

Liang J, Balachandra S, Ngo S, and O'Brien LE (2017). Feedback regulation of steady-state epithelial turnover and organ size. Nature 548, 588–591. [PubMed: 28847000]

Lin G, Xu N, and Xi R (2008). Paracrine Wingless signalling controls self-renewal of Drosophila intestinal stem cells. Nature 455, 1119–1123. [PubMed: 18806781]

Lin G, Xu N, and Xi R (2010). Paracrine unpaired signaling through the JAK/STAT pathway controls self-renewal and lineage differentiation of Drosophila intestinal stem cells. J. Mol. Cell Biol 2, 37–49. [PubMed: 19797317]

Lucchetta EM, and Ohlstein B (2012). The Drosophila midgut: a model for stem cell driven tissue regeneration. Wiley Interdiscip. Rev. Dev. Biol 1, 781–788. [PubMed: 23799573]

Makhijani K, Alexander B, Tanaka T, Rulifson E, and Brückner K (2011). The peripheral nervous system supports blood cell homing and survival in the Drosophila larva. Development 138, 5379–5391. [PubMed: 22071105]

Martín FA, Peréz-Garijo A, and Morata G (2009). Apoptosis in Drosophila: compensatory proliferation and undead cells. Int. J. Dev. Biol 53, 1341–1347. [PubMed: 19247932]

Mathur D, Bost A, Driver I, and Ohlstein B (2010). A transient niche regulates the specification of Drosophila intestinal stem cells. Science 327, 210–213. [PubMed: 20056890]

McGuire SE, Le PT, Osborn AJ, Matsumoto K, and Davis RL (2003). Spatiotemporal rescue of memory dysfunction in Drosophila. Science 302, 1765–1768. [PubMed: 14657498]

Micchelli CA, and Perrimon N (2006). Evidence that stem cells reside in the adult Drosophila midgut epithelium. Nature 439, 475–479. [PubMed: 16340959]

Miguel-Aliaga I, Jasper H, and Lemaitre B (2018). Anatomy and Physiology of the Digestive Tract of *Drosophila melanogaster*. Genetics 210, 357–396. [PubMed: 30287514]

Mollereau B, Perez-Garijo A, Bergmann A, Miura M, Gerlitz O, Ryoo HD, Steller H, and Morata G (2013). Compensatory proliferation and apoptosis-induced proliferation: a need for clarification. Cell Death Differ 20, 181. [PubMed: 22722336]

Morris O, Liu X, Domingues C, Runchel C, Chai A, Basith S, Tenev T, Chen H, Choi S, Pennetta G, et al. (2016). Signal Integration by the IkB Protein Pickle Shapes Drosophila Innate Host Defense. Cell Host Microbe 20, 283–295. [PubMed: 27631699]

Muzzopappa M, Murcia L, and Milán M (2017). Feedback amplification loop drives malignant growth in epithelial tissues. Proc. Natl. Acad. Sci. USA 114, E7291–E7300. [PubMed: 28808034]

O'Brien LE, Soliman SS, Li X, and Bilder D (2011). Altered modes of stem cell division drive adaptive intestinal growth. Cell 147, 603–614. [PubMed: 22036568]

Ohlstein B, and Spradling A (2006). The adult Drosophila posterior midgut is maintained by pluripotent stem cells. Nature 439, 470–474. [PubMed: 16340960]

Ohlstein B, and Spradling A (2007). Multipotent Drosophila intestinal stem cells specify daughter cell fates by differential notch signaling. Science 315, 988–992. [PubMed: 17303754]

Osman D, Buchon N, Chakrabarti S, Huang YT, Su WC, Poidevin M, Tsai YC, and Lemaitre B (2012). Autocrine and paracrine unpaired signaling regulate intestinal stem cell maintenance and division. J. Cell Sci. 125, 5944–5949. [PubMed: 23038775]

Patel PH, Pénalva C, Kardorff M, Roca M, Pavlović B, Thiel A, Teleman AA, and Edgar BA (2019). Damage sensing by a Nox-Ask1-MKK3-p38 signaling pathway mediates regeneration in the adult Drosophila midgut. Nat. Commun 10, 4365. [PubMed: 31554796]

Pérez E, Lindblad JL, and Bergmann A (2017). Tumor-promoting function of apoptotic caspases by an amplification loop involving ROS, macrophages and JNK in *Drosophila*. eLife 6, e26747. [PubMed: 28853394]

Pérez-Garijo A, Martín FA, and Morata G (2004). Caspase inhibition during apoptosis causes abnormal signalling and developmental aberrations in Drosophila. Development 131, 5591–5598. [PubMed: 15496444]

Ray PD, Huang BW, and Tsuji Y (2012). Reactive oxygen species (ROS) homeostasis and redox regulation in cellular signaling. Cell. Signal 24, 981–990. [PubMed: 22286106]

Ren F, Wang B, Yue T, Yun EY, Ip YT, and Jiang J (2010). Hippo signaling regulates Drosophila intestine stem cell proliferation through multiple pathways. Proc. Natl. Acad. Sci. USA 107, 21064–21069. [PubMed: 21078993]

Ring JM, and Martinez Arias A (1993). puckered, a gene involved in position-specific cell differentiation in the dorsal epidermis of the Drosophila larva. Development Suppl, 251–259.

Ryoo HD, Gorenc T, and Steller H (2004). Apoptotic cells can induce compensatory cell proliferation through the JNK and the Wingless signaling pathways. Dev. Cell 7, 491–501. [PubMed: 15469838]

Salvesen GS, Hempel A, and Coll NS (2016). Protease signaling in animal and plant-regulated cell death. FEBS J 283, 2577–2598. [PubMed: 26648190]

Santabárbara-Ruiz P, Esteban-Collado J, Pérez L, Viola G, Abril JF, Milán M, Corominas M, and Serras F (2019). Ask1 and Akt act synergistically to promote ROS-dependent regeneration in Drosophila. PLoS Genet 15, e1007926. [PubMed: 30677014]

Schieber M, and Chandel NS (2014). ROS function in redox signaling and oxidative stress. Curr. Biol 24, R453–R462. [PubMed: 24845678]

Shalini S, Dorstyn L, Dawar S, and Kumar S (2015). Old, new and emerging functions of caspases. Cell Death Differ 22, 526–539. [PubMed: 25526085]

Sinenko SA, and Mathey-Prevot B (2004). Increased expression of Drosophila tetraspanin, Tsp68C, suppresses the abnormal proliferation of ytr-deficient and Ras/Raf-activated hemocytes. Oncogene 23, 9120–9128. [PubMed: 15480416]

Spéder P, Adám G, and Noselli S (2006). Type ID unconventional myosin controls left-right asymmetry in Drosophila. Nature 440, 803–807. [PubMed: 16598259]

Staley BK, and Irvine KD (2010). Warts and Yorkie mediate intestinal regeneration by influencing stem cell proliferation. Curr. Biol 20, 1580–1587. [PubMed: 20727758]

Sykiotis GP, and Bohmann D (2008). Keap1/Nrf2 signaling regulates oxidative stress tolerance and lifespan in Drosophila. Dev. Cell 14, 76–85. [PubMed: 18194654]

Tang HL, Tang HM, Fung MC, and Hardwick JM (2015). In vivo CaspaseTracker biosensor system for detecting anastasis and non-apoptotic caspase activity. Sci. Rep 5, 9015. [PubMed: 25757939]

Tian A, and Jiang J (2014). Intestinal epithelium-derived BMP controls stem cell self-renewal in Drosophila adult midgut. eLife 3, e01857. [PubMed: 24618900]

Tian A, Benchabane H, Wang Z, and Ahmed Y (2016). Regulation of Stem Cell Proliferation and Cell Fate Specification by Wingless/Wnt Signaling Gradients Enriched at Adult Intestinal Compartment Boundaries. PLoS Genet 12, e1005822. [PubMed: 26845150]

Wilson R, Goyal L, Ditzel M, Zachariou A, Baker DA, Agapite J, Steller H, and Meier P (2002). The DIAP1 RING finger mediates ubiquitination of Dronc and is indispensable for regulating apoptosis. Nat. Cell Biol 4, 445–450. [PubMed: 12021771]

Xu N, Wang SQ, Tan D, Gao Y, Lin G, and Xi R (2011). EGFR, Wingless and JAK/STAT signaling cooperatively maintain Drosophila intestinal stem cells. Dev. Biol 354, 31–43. [PubMed: 21440535]

Yagi Y, and Hayashi S (1997). Role of the Drosophila EGF receptor in determination of the dorsoventral domains of escargot expression during primary neurogenesis. Genes Cells 2, 41–53. [PubMed: 9112439]

Zeng X, Chauhan C, and Hou SX (2010). Characterization of midgut stem cell- and enteroblast-specific Gal4 lines in Drosophila. Genesis 48, 607–611. [PubMed: 20681020]

Zhou F, Rasmussen A, Lee S, and Agaisse H (2013). The UPD3 cytokine couples environmental challenge and intestinal stem cell division through modulation of JAK/STAT signaling in the stem cell microenvironment. Dev. Biol 373, 383–393. [PubMed: 23110761]

Zhou J, Florescu S, Boettcher AL, Luo L, Dutta D, Kerr G, Cai Y, Edgar BA, and Boutros M (2015). Dpp/Gbb signaling is required for normal intestinal regeneration during infection. Dev. Biol 399, 189–203. [PubMed: 25553980]

Highlights

- *Myo1D* mutants display reduced rates of mitosis in the adult midgut
- Myo1D controls ISC activity non-autonomously from ECs
- Myo1D translocates Dronc to the basal side of the plasma membrane of enterocytes
- Several signaling pathways have reduced activity in *Myo1D* mutants

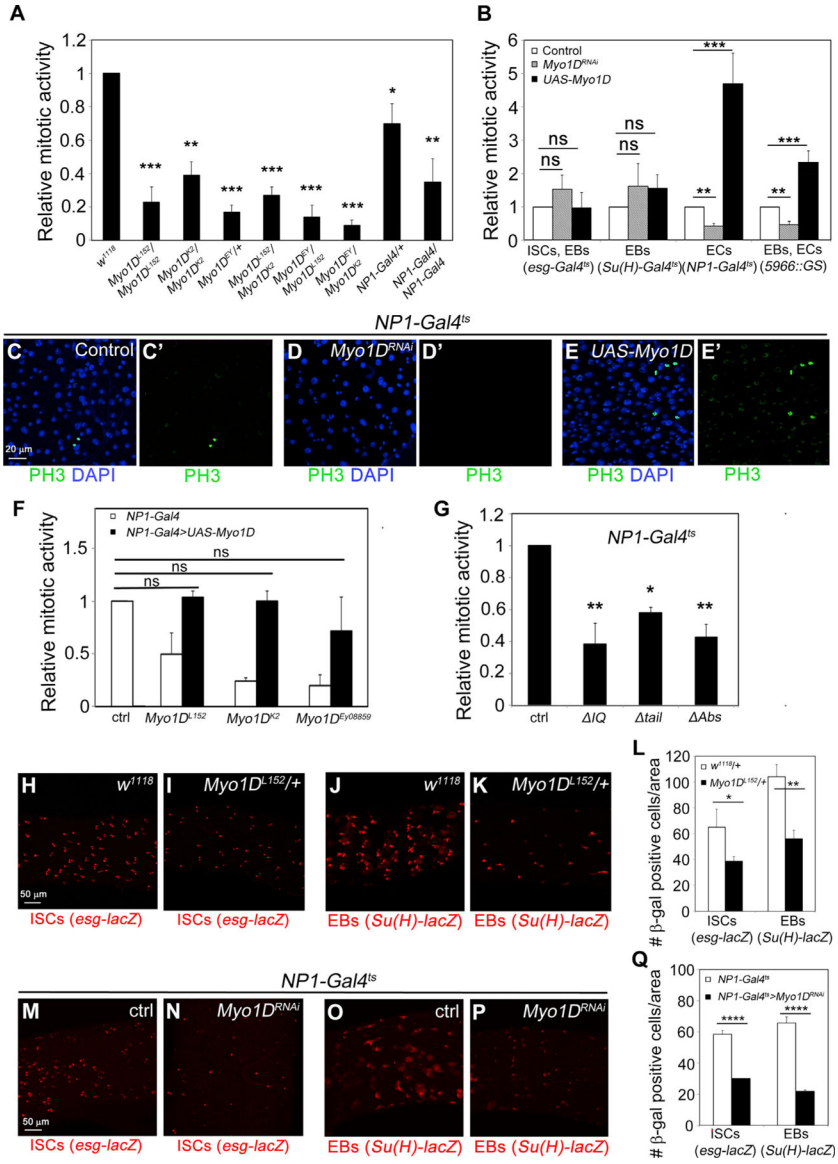

Figure 1. *Myo1D* Is Non-Cell-Autonomously Required for Mitotic Activity of ISCs

(A) *Myo1D* is partially required for mitotic activity of ISCs. Various allelic combinations of *Myo1D* mutants were tested. Mitotic activity was determined by PH3 labelings. Even heterozygous *Myo1D* mutants display reduced mitotic activity. $Myo1D^{EY}$ is $Myo1D^{EY08859}$. *NP1-Gal4* is a Gal4 insertion in the *Myo1D* gene and a partial loss-of-function mutant. PH3 counts were analyzed by ordinary one-way ANOVA for multiple comparisons. Plotted is relative mitotic activity ± SEM. ***p < 0.001; **p < 0.01; *p < 0.05. p values are relative to w^{1118}.

(B) *Myo1D* controls mitotic activity of ISCs in ECs. *esg-Gal4* and *Su(H)-Gal4* are expressed in progenitor cells; *NP1-Gal4* and 5966::GS are expressed in ECs. Controls are the Gal4 drivers over +. In this and the following figures, the ^{ts} annotation indicates the *tub-Gal80*^{ts} transgene for temporal control of Gal4 activity. Conditional expression from the *5966::GS* driver was induced by feeding RU486 to the animals. PH3 counts were analyzed by ordinary

one-way ANOVA for multiple comparisons. Plotted is relative mitotic activity ± SEM. **p < 0.01; ***p < 0.001. ns, not significant.

(C–E) Representative examples of PH3 (green) labelings in posterior midguts with either normal (C), reduced (D), or increased (E) levels of *Myo1D*. DAPI (blue) labels nuclei.

(F) Expression of a wild-type *UAS-Myo1D* transgene in ECs using *NP1-Gal4* can rescue the ISC mitotic phenotype of the indicated *Myo1D* mutants. Please note that *NP1-Gal4* itself is a loss-of-function allele of *Myo1D*. Therefore, the *Myo1D* mutants are trans-heterozygous with *NP1-Gal4*. Control (ctrl) is *NP1-Gal4*/+. PH3 counts were analyzed by ordinary one-way ANOVA for multiple comparisons. Plotted is relative mitotic activity ± SEM. ns, not significant.

(G) Several upstream activating sequence (UAS)-based transgenes encoding mutant forms of *Myo1D* (*Myo1D*$^{\Delta IQ}$, *Myo1D*$^{\Delta tail}$, *Myo1D*$^{\Delta Abs}$) are dominant-negative alleles. Control (ctrl) is *NP1-Gal4*/+. PH3 counts were analyzed by ordinary one-way ANOVA for multiple comparisons. Plotted is relative mitotic activity ± SEM. *p < 0.05; **p < 0.01. p values are relative to ctrl.

(H–K) Heterozygosity of the amorphic *Myo1D*^{L152} allele results in partial loss of precursor cells, labeled by *esg-lacZ* for ISCs (H and I) and *Su(H)-lacZ* for EBs (J and K).

(L) Quantification of (H)–(K). β-Gal positive cells were analyzed by unpaired t test, two tailored, and plotted ± SEM. *p < 0.05; **p < 0.01.

(M–P) Depletion of *Myo1D* by RNAi results in partial loss of precursor cells, labeled by *esg-lacZ* for ISCs (M and N) and *Su(H)-lacZ* for EBs (O and P).

(Q) Quantification of (M)–(P). β-Gal positive cells were analyzed by unpaired t test, two tailored, and plotted ± SEM. ****p < 0.0001.

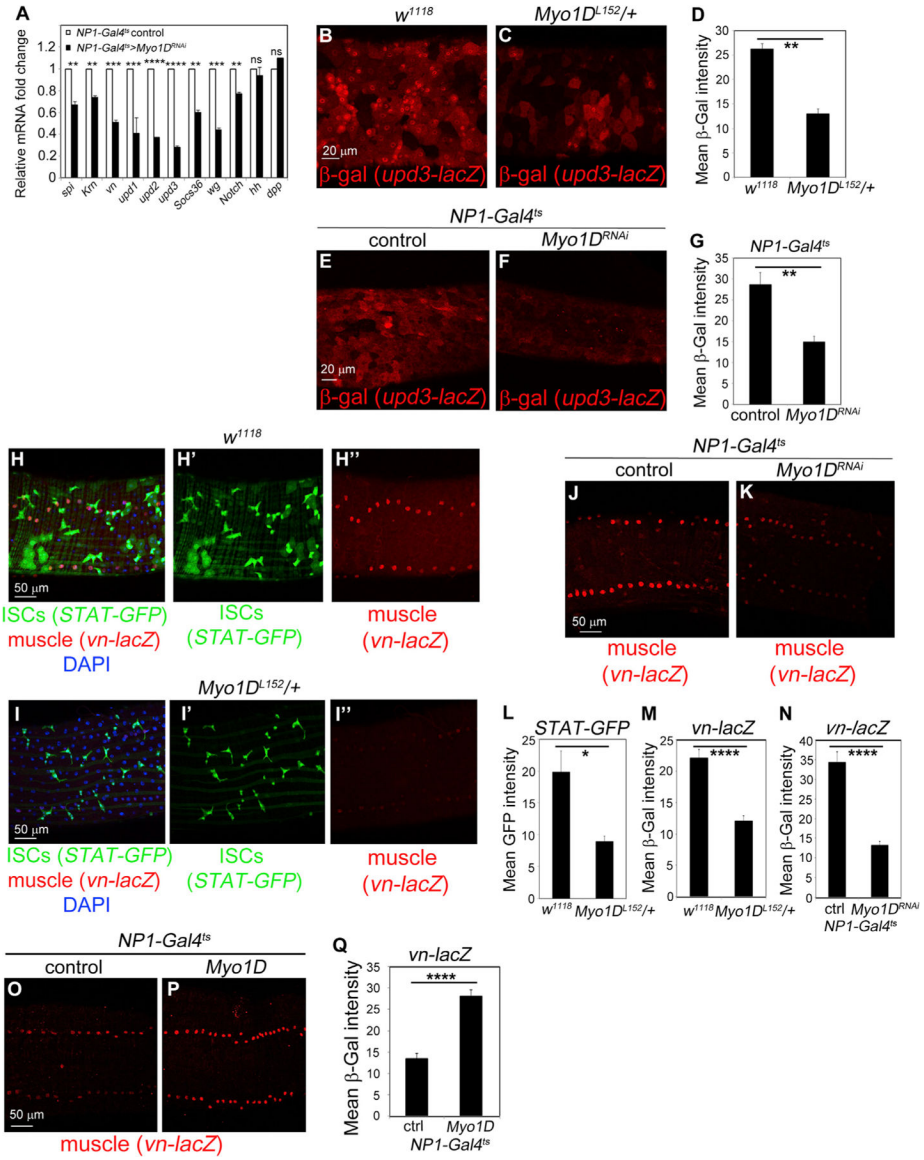

Figure 2. *Myo1D* Is Required for Various Signaling Events between ECs and Stem Cells/Muscle Cells

(A) qRT-PCR analysis of the expression of select signaling genes in the midgut as a function of EC-specific *Myo1D* RNAi. Primer sequences are listed in Table S1. The values for pairwise comparisons (control versus *Myo1D* RNAi) were analyzed by unpaired t test, two tailored. Plotted is mean signal ± SEM. **p < 0.01; ***p < 0.001; ****p < 0.0001. ns, not significant.

(B and C) The amorphic $Myo1D^{L152}$ allele dominantly affects *upd3-lacz* expression.

(D) Quantification of (B) and (C). β-Gal signal intensities were determined and analyzed by unpaired t test, two-tailored. Plotted is mean intensity ± SE. **p < 0.01.

(E and F) Depletion of *Myo1D* by RNAi partially impairs *upd3-lacZ* expression. Control is *NP1-Gal4*/+.

(G) Quantification of (E) and (F). β-Gal signal intensities were determined and analyzed by unpaired t test, two-tailored. Plotted is mean intensity ± SEM. **p < 0.01.

(H–I′′) ISC-specific STAT activity (*STAT-GFP*) and muscle-specific *vein* (*vn-lacZ*) expression is partially dependent on *Myo1D*. Quantified in (L) (*STAT-GFP*) and (M) (*vn-lacZ*).

(J and K) EC-specific knockdown of *Myo1D* affects *vein* expression (*vn-lacZ*) in the visceral muscle. Quantified in (N).

(L–N) Quantification of the data shown in (H)–(K). All three datasets were analyzed by unpaired t test, two tailored. In the case of *STAT-GFP* (H′ and I′), mean signal intensities were determined and plotted ± SEM (L). In the case of *vn-lacZ* (H′′, I′′, J, and K), mean β-Gal signal intensities per nucleus were determined and plotted ± SEM. *$p < 0.05$; ****$p < 0.0001$.

(O and P) Muscle-specific *vn-lacZ* expression is strongly induced by EC-specific overexpression of *Myo1D*.

(Q) Quantification of (O) and (P). β-Gal signal intensities per nucleus were determined and analyzed by unpaired t test, two-tailored. Plotted is mean intensity ± SEM. ****$p < 0.0001$. See also Table S1.

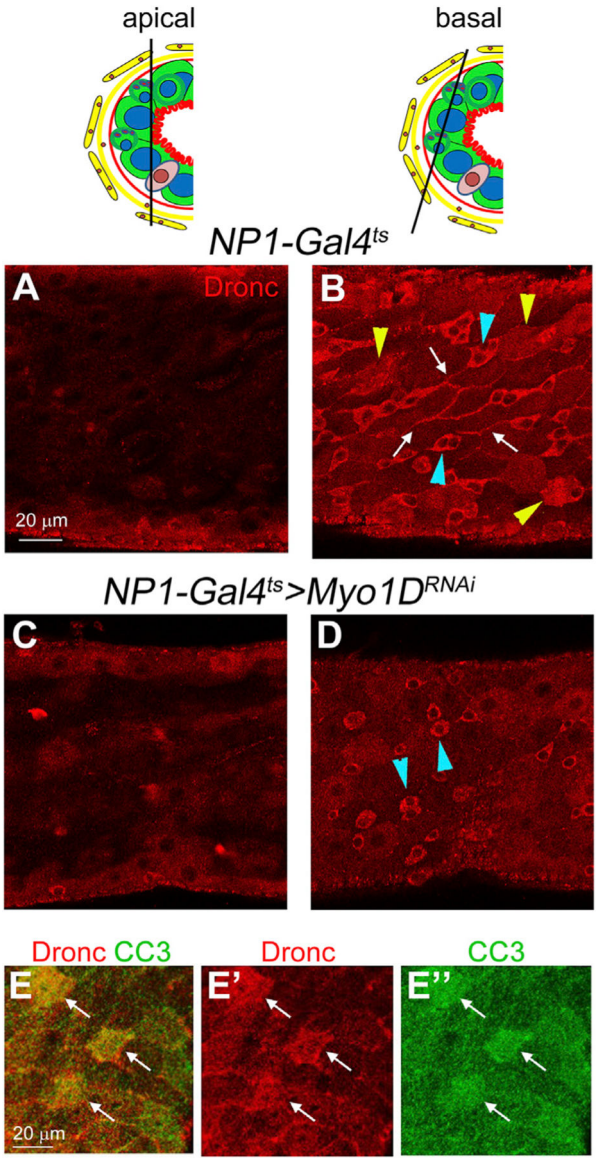

Figure 3. *Myo1D* Is Required for Dronc Localization to the Basal Side of the Plasma Membrane in ECs

(A–D) Analysis of the subcellular localization of Dronc protein in the posterior midgut. The schemes above the panels indicate the focal plane across the midgut (apical [A and C] or basal [B and D]), which was applied when the midgut labelings were imaged (black line). White arrows in (B) point to ECs with plasma membrane localization of Dronc; yellow arrowheads point to ECs with cytosolic Dronc. Blue arrowheads in (B) and (D) point to the smaller precursor cells. (C and D) EC-specific knockdown of *Myo1D* by *NP1-Gal4*^{ts}. The membrane localization of Dronc in ECs is lost.

(E) ECs with high levels of cytosolic Dronc are apoptotic as judged by the CC3 antibody. White arrows indicate examples.

See also Figures S1 and S2.

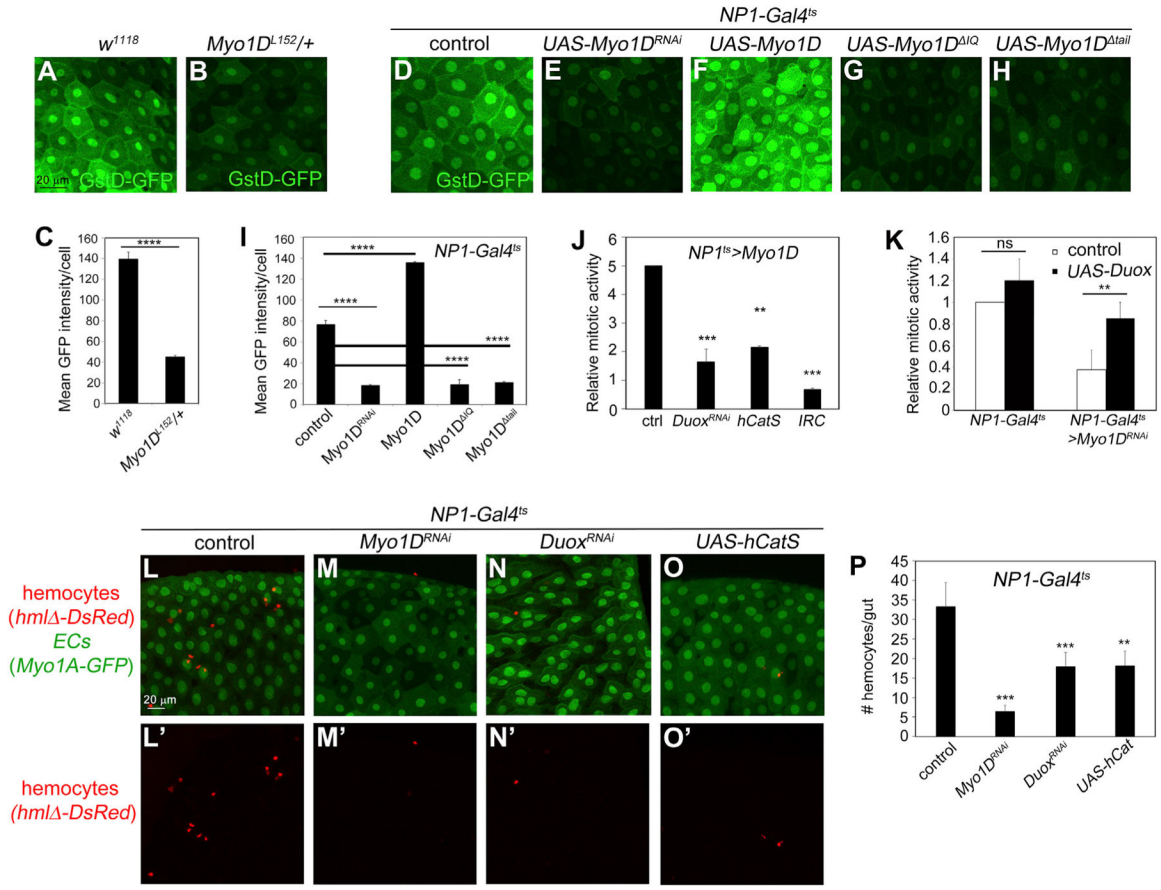

Figure 4. *Myo1D* Is Required for ROS Generation and Hemocyte Recruitment to the Midgut

(A and B) The amorphic *Myo1D*^{L152} allele dominantly reduces the redox-reporter *GstD-GFP*.

(C) Quantification of (A) and (B). GFP signal intensities were determined and analyzed by unpaired t test, two-tailored. Plotted is mean intensity ± SEM. ****p < 0.0001.

(D–H) Analysis of the redox-reporter *GstD-GFP* in response to knockdown (E) or overexpression of *Myo1D* (F) and the dominant-negative *Myo1D*$^{\Delta IQ}$ (G) and *Myo1D*$^{\Delta tail}$ (H) transgenes. Control is *NP1-Gal4*/+.

(I) Quantification of (D)–(H). GFP signal intensities were determined in defined areas and analyzed by ordinary one-way ANOVA. Plotted is mean intensity ± SEM. ****p < 0.0001.

(J) *Myo1D*-induced mitotic activity of ISCs is dependent on extracellular ROS. *Duox* RNAi and overexpression of extracellular catalases *hCatS* (human secreted catalase) and *IRC*. Control (ctrl) is *NP1-Gal4*/+. PH3 counts were analyzed by ordinary one-way ANOVA for multiple comparisons. Plotted is relative mitotic activity ± SEM. **p < 0.01; ***p < 0.001.

(K) The reduction of the mitotic activity caused by *Myo1D* RNAi can be partially rescued by overexpression of *Duox*. PH3 counts in the two datasets were analyzed by unpaired t test, two tailored. Plotted is relative mitotic activity ± SEM. **p < 0.01. ns – not significant.

(L–O) Recruitment of hemocytes to the midgut is dependent on *Myo1D* and ROS. Depletion of *Myo1D* (M) and *Duox* (N) by RNAi as well as reduction of extracellular ROS by overexpression of *hCatS* partially reduces the recruitment of hemocytes to the midgut. A *hmlΔ-DsRed* transgene was used to label hemocytes. Control: *NP1-Gal4*/+.

(P) Quantification of (L)–(O). Hemocyte counts were analyzed by ordinary one-way ANOVA for multiple comparisons. Plotted is number of hemocytes per gut ± SEM. **p < 0.01; ***p < 0.001.

See also Figure S3.

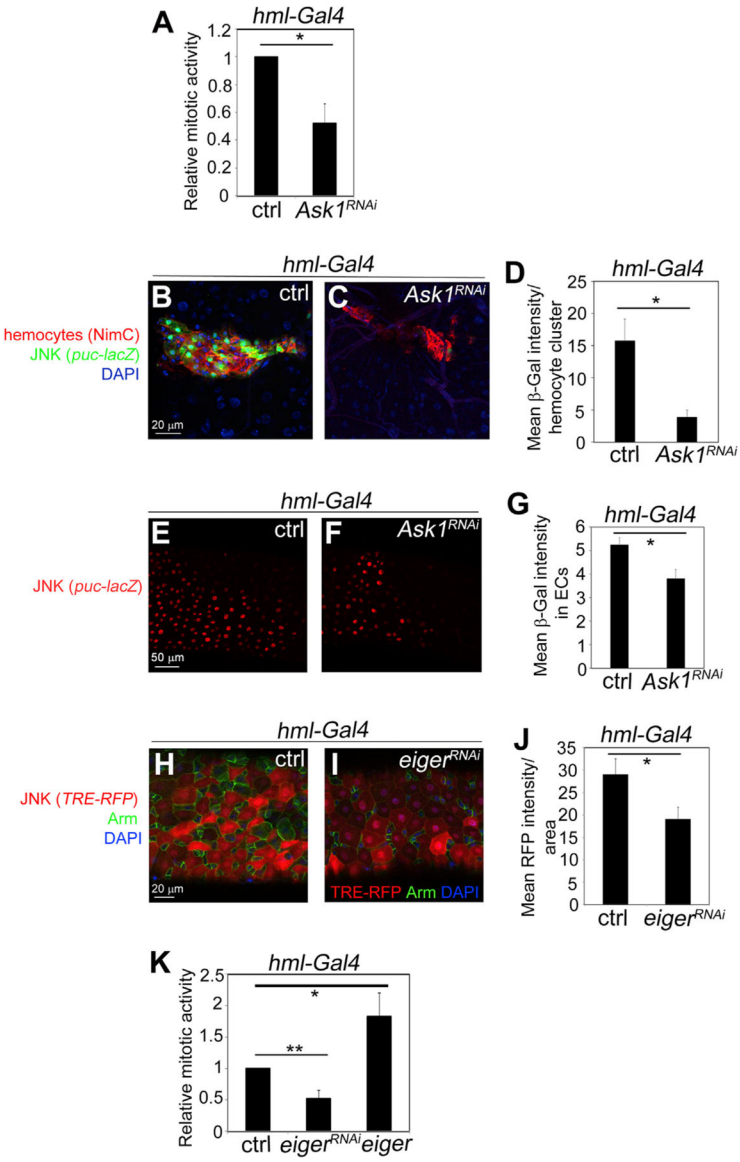

Figure 5. JNK Activity Is Induced in Both Hemocytes and ECs

hmlΔ-Gal4 drives expression of UAS-based transgenes specifically in hemocytes.

(A) Hemocyte-specific knockdown of *Ask1* partially reduces ISC mitotic activity. PH3 counts were analyzed by unpaired t test with Welch's correction, two tailored, and plotted as relative mitotic activity ± SEM. *p < 0.05.

(B and C) JNK activity is induced in hemocytes. Shown are confocal images focusing on the surface of the midgut where hemocytes are attached. The NimC antibody labels hemocytes (red); β-Gal labeling (green) detects the JNK marker *puc-lacZ*. Normal hemocytes are β-Gal positive, suggesting that they contain active JNK (B). Hemocyte-specific depletion of *Ask1* results in loss of JNK activity (C).

(D) Quantification of (B) and (C). β-Gal intensity was determined in hemocyte clusters and analyzed by unpaired t test with Welch's correction, two tailored. Plotted is mean intensity per cluster ± SEM. *p < 0.05.

(E and F) Shown are confocal images focusing on ECs in the midgut. *puc-lacZ* is a marker of JNK activity. Hemocyte-specific depletion of *Ask1* results in partial loss of JNK activity in ECs.

(G) Quantification of (E) and (F). β-Gal intensity in ECs was analyzed by unpaired t test, two tailored. Plotted is mean intensity in ECs ± SEM. *$p < 0.05$.

(H and I) Hemocyte-specific knockdown of *eiger* results in partial loss of JNK activity in ECs. JNK activity was detected using tetradecanoylphorbol acetate response element-red fluorescent protein (*TRE-RFP*).

(J) Quantification of (H) and (I). RFP intensity was determined in defined areas and analyzed by unpaired t test, two tailored. Plotted is mean intensity per area ± SEM. *$p < 0.05$.

(K) Hemocyte-specific loss (by RNAi) or increase (by *UAS-eiger*) of *eiger* reduces or increases the mitotic activity of ISCs, respectively. PH3 counts were analyzed by ordinary one-way ANOVA and plotted as relative mitotic activity ± SEM. *$p < 0.05$; **$p < 0.01$. See also Figure S4.

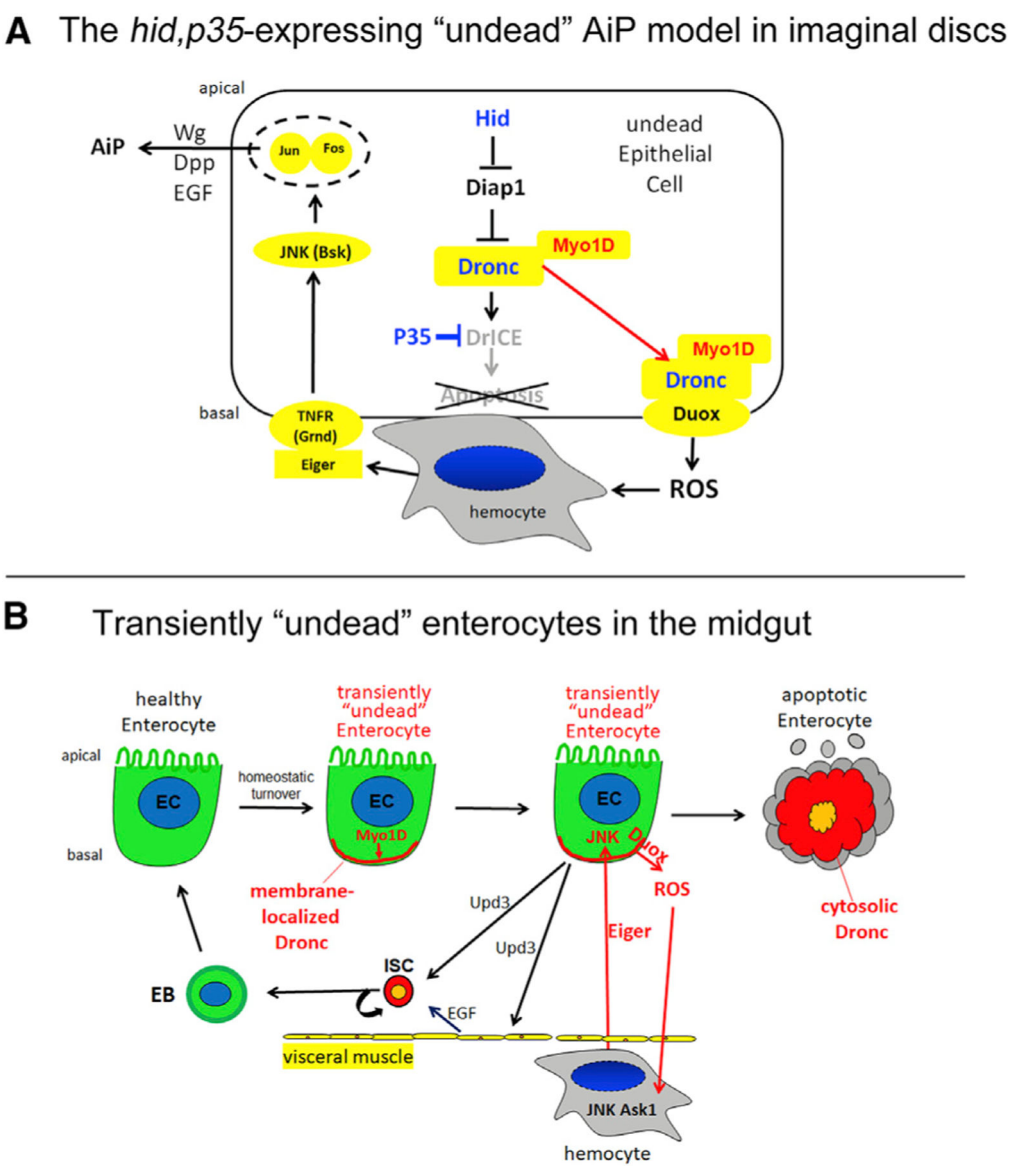

Figure 6. Comparison of Undead AiP in Imaginal Discs and the Role of Transiently Undead ECs for Homeostatic Turnover in the Adult Posterior Midgut

(A) The *hid,p35*-expressing undead AiP model in larval imaginal discs. Myo1D has a key role by localizing Dronc to the basal side of the plasma membrane in close proximity to the NADPH oxidase Duox. ROS generated by Duox attract hemocytes, which release Eiger and trigger JNK signaling in undead cells. This leads to the production of the mitogens Wg, Dpp, and EGF (Spi) for AiP. Please note the apical-basal polarity of these cells.

(B) Transiently undead ECs in the adult posterior midgut. Relevant parts are presented in red. Please note the similarities to the undead AiP model in imaginal discs (A). When ECs are getting ready for turnover, Dronc (red) is localized to the basal side of the plasma membrane in a *Myo1D*-dependent manner, rendering ECs transiently undead. Dronc stimulates Duox activity for ROS generation, hemocyte recruitment, and JNK activation in hemocytes and undead ECs. That releases Upd3 for stimulation of mitotic activity of ISCs.

After that, undead ECs release Dronc from the membrane and become apoptotic. Please note that ISCs and visceral muscle cells are in direct contact with the basal side of ECs.
See also Figure S5.

KEY RESOURCES TABLE

REAGENT or RESOURCE	SOURCE	IDENTIFIER
Antibodies		
Mouse monoclonal anti-β-Galactosidase	Developmental Studies Hybridoma Bank (DSHB)	cat#40-1a
Rabbit polyclonal anti-cleaved Caspase-3 (Asp175) (5A1E) Rabbit mAb	Cell Signaling Technology	cat#9664; RRID: AB_2341188
Mouse monoclonal anti-NimC antibody	Dr. Istvan Ando	RRID: AB_2568423 Kurucz et al., 2007
Guinea pig polyclonal anti-Dronc antibody	Dr. Pascal Meier	SK11 Wilson et al., 2002
Rabbit monoclonal phospho-histone H3 (PH3)	Millipore	cat#17-10141
Chemicals, Peptides, and Recombinant Proteins		
Dihydroethidium (DHE)	Invitrogen	Cat#D23107
Vectorshield with DAPI	Vector Laboratories	Cat#H-1200; RRID: AB_2336790
Experimental Models: Organisms/Strains		
Drosophila melanogaster: *Myo1D*^{EY08859}	Bloomington *Drosophila* Stock Center	BDSC 19940; FlyBase:FBal0160157
Drosophila melanogaster: *UAS-Myo1D*	Kenji Matsuno	FlyBase: FBal0280076; (Hozumi et al., 2008)
Drosophila melanogaster: *UAS-Myo1D*$^{\Delta Abs}$	Kenji Matsuno	FlyBase: FBal0280079; (Hozumi et al., 2008)
Drosophila melanogaster: *UAS-Myo1D*$^{\Delta IQ}$	Kenji Matsuno	FlyBase: FBal0280080; (Hozumi et al., 2008)
Drosophila melanogaster: *UAS-Myo1D*$^{\Delta tail}$	Kenji Matsuno	FlyBase: FBal0280081; (Hozumi et al., 2008)
Drosophila melanogaster: *UAS-Myo1D* RNAi	Bloomington *Drosophila* Stock Center	BDSC 33971; FlyBase: FBal0257601
Drosophila melanogaster: *UAS-Myo1D* RNAi	Vienna *Drosophila* Resource Center	VDRC v102456; FlyBase: FBal0231812
Drosophila melanogaster: *esg-Gal4*	Y. Tony Ip	FlyBase: FBal0299620 (Yagi and Hayashi, 1997)
Drosophila melanogaster: *Su(H)GBE-Gal4*	Y. Tony Ip	BDSC: 83377 FlyBase: FBst0083377 (Zeng et al., 2010)
Drosophila melanogaster: NP1-Gal4	Bruce Edgar	FlyBase: FBal0256622 (Jiang and Edgar, 2009)
Drosophila melanogaster: *5966::GS*	Benjamin Ohlstein	FlyBase: FBti0150384 (Mathur et al., 2010)
Drosophila melanogaster: *Su(H)-lacZ*	Y. Tony Ip	(Furriols and Bray, 2001)
Drosophila melanogaster: *hmlΔ-Gal4*	Katja Brueckner	BDSC: 30139 FlyBase: FBst0030139 (Sinenko and Mathey-Prevot, 2004)
Drosophila melanogaster: *hmlΔ-Gal4*	Katja Brueckner	BDSC: 30141 FlyBase: FBst0030141 (Sinenko and Mathey-Prevot, 2004)
Drosophila melanogaster: *hmlΔ-DsRed*	Katja Brueckner	FlyBase: FBtp0141955 (Makhijani et al., 2011)
Drosophila melanogaster: *esg-lacZ*	Y. Tony Ip	Flybase: FBti0003318
Drosophila melanogaster: *GstD-GFP*	Dirk Bohmann	FlyBase: FBtp0069371 (Sykiotis and Bohmann, 2008)
Drosophila melanogaster: TRE-RFP	Dirk Bohmann	BDSC: 59011 FlyBase: FBst0059011 (Chatterjee and Bohmann, 2012)
Drosophila melanogaster: TRE-RFP	Dirk Bohmann	BDSC: 59012 FlyBase: FBst0059012 (Chatterjee and Bohmann, 2012)
Drosophila melanogaster: CaspaseTracker	Marie Hardwick	(Tang et al., 2015)
Drosophila melanogaster: *msn-lacZ*	Bloomington *Drosophila* Stock Center	BDSC 11707 FlyBase: FBti0005574
Drosophila melanogaster: *upd3-lacZ*	Y. Tony Ip	FlyBase: FBtp0113439 (Zhou et al., 2013)
Drosophila melanogaster: *STAT-GFP*	Erika Bach	FlyBase: FBtp0036827 (Bach et al., 2007)

REAGENT or RESOURCE	SOURCE	IDENTIFIER
Drosophila melanogaster: *vn-lacZ*	Bloomington *Drosophila* Stock Center	FlyBase: FBst0011749 BDSC 11749
Drosophila melanogaster: *UAS-Duox* RNAi	Won-Jae Lee	FlyBase:FBal0190061; Ha et al., 2005a
Drosophila melanogaster: *UAS-IRC*	Won-Jae Lee	FlyBase: FBal0191070; Ha et al., 2005b
Drosophila melanogaster:*UAS-hCatS*	Won-Jae Lee	FlyBase: FBtp0020737; Ha et al., 2005b
Drosophila melanogaster: *UAS-dAsk1*	Bloomington *Drosophila* Stock Center	FlyBase: FBti0132158; BDSC 32464
Drosophila melanogaster: *UAS-Eiger* RNAi	Masayuki Miura	FlyBase: FBal0147162; (Igaki et al., 2002)
Drosophila melanogaster: *UAS-Dronc* RNAi	Vienna *Drosophila* Resource Center	FlyBase: FBst0472297; VDRC v100424;
Drosophila melanogaster: *UAS-Dronc*	Andreas Bergmann	FlyBase:FBal0326367; (Kamber Kaya et al., 2017)
Drosophila melanogaster: *tub-Gal80^{ts}*	Bloomington Drosophila Stock Center	FlyBase: FBti0027796; BDSC 7019 (McGuire et al., 2003)
Drosophila melanogaster: UAS-hid;ey-Gal4 UAS-p35/CyO,tub-Gal80	Andreas Bergmann	(Fan et al., 2014)
Drosophila melanogaster: ey-Gal4 UAS-p35/CyO	Andreas Bergmann	(Fan et al., 2014)
Drosophila melanogaster: *Myo1D^{L152}*	Kenji Matsuno	FlyBase: FBal0195152; (Hozumi et al., 2006)
Drosophila melanogaster: *Myo1D^{K2}*	Stephane Noselli	FlyBase:FBal0194493; (Spéder et al., 2006)
Drosophila melanogaster; *puc^{E69}* (*puc-lacZ*)	N/A	FlyBase:FBal0047865 Ring and Martinez Arias, 1993
Oligonucleotides		
	See Table S1	N/A
Software and Algorithms		
Photoshop	Adobe	Version 5.5
GraphPad Prism Software	GraphPad	Version 7.04
Zen imaging software	Carl Zeiss AG	Version 3.1